

Monte Carlo Simulations of the two-dimensional dipolar fluid

Jean-Michel Caillol* and Jean-Jacques Weis†

Univ. Paris-Sud, CNRS, LPT, UMR 8627, Orsay, F-91405, France

Abstract

We study a two-dimensional fluid of dipolar hard disks by Monte Carlo simulations in a square with periodic boundary conditions and on the surface of a sphere. The theory of the dielectric constant and the asymptotic behaviour of the equilibrium pair correlation function in the fluid phase is derived for both geometries. After having established the equivalence of the two methods we study the stability of the liquid phase in the canonical ensemble. We give evidence of a phase made of living polymers at low temperatures and provide a tentative phase diagram.

Keywords: Two-dimensional dipolar fluid; Monte Carlo simulations; Periodic Boundary conditions; Spherical boundary conditions.

*Electronic address: Jean-Michel.Caillol@th.u-psud.fr

†Electronic address: Jean-Jacques.Weis@th.u-psud.fr

I. INTRODUCTION

This paper is devoted to a study of a two-dimensional (2D) system made of identical dipolar hard disks (DHD) in the Euclidian plane E_2 by means of Monte-Carlo (MC) simulations. The dipoles are assumed to be permanent and the configurational energy of N dipolar molecules in E_2 reads as

$$H = \frac{1}{2} \sum_{i \neq j}^N v_{HS}(r_{ij}) + \frac{1}{2} \mu^2 \sum_{i \neq j}^N \frac{1}{r_{ij}^2} \left[\mathbf{s}_i \cdot \mathbf{s}_j - \frac{2(\mathbf{s}_i \cdot \mathbf{r}_{ij})(\mathbf{s}_j \cdot \mathbf{r}_{ij})}{r_{ij}^2} \right] \quad (1)$$

In Eq. (1), $v_{HS}(r)$ is the hard disk potential of diameter σ . The second term is the contribution from the 2D dipole-dipole interaction where $\boldsymbol{\mu}_i = \mu \mathbf{s}_i$, μ permanent dipole moment, \mathbf{s}_i unit vector in the direction of the dipole moment of particle i , $\mathbf{r}_{ij} = \mathbf{r}_j - \mathbf{r}_i$, the vector joining the centres of mass of the particles, and $r_{ij} = |\mathbf{r}_{ij}|$. We stress that the system that we consider cannot be seen as a thin layer of a real 3D system of dipoles. In this case, the electrostatic interactions should be derived from the solutions of the 3D Laplace equation while the dipole-dipole interaction involved in Eq. (1) is derived from the solution of the 2D Laplace equation in the plane.

We have performed MC simulations of the DHD fluid in a square with periodic boundary conditions and on the surface of an ordinary sphere. In both cases the dipole-dipole interaction is obtained from a rigorous solution of Laplace equation in the considered geometry [1–4]. We compare the two methods in the liquid phase and check that they both yield the same thermodynamic, structural and dielectric properties. Both methods are then used for preliminaries MC studies of the DHD fluid at low temperatures. In this regime, as for real 3D dipoles confined in a plane (see *e.g.*, Ref. [5]), the 2D dipoles aggregate to form living chains and ring polymers at low densities and more involved structures at higher densities.

The paper is organized as follows. After this introduction we give details on the two simulation techniques used in this work in Sec. II. Next Sec. III is devoted to a digest of the general theory of dielectric media in an arbitrary 2D geometry [4], with applications to the square with periodic boundary conditions and the sphere. This theoretical analysis is notably required to understand the long range tails of the pair correlation functions in both geometries. Checks of these asymptotic behaviours as well as quantitative comparisons

between the two methods are discussed in Sec. IV. In Sec. V we present extensive MC simulations of the DHD fluid by both methods and give a tentative phase diagram of the system. We conclude in Sec. VI

II. SIMULATION METHODS

A. Periodic boundary conditions

In this method the simulation cell is a square of side L with periodic boundary conditions, that will be referred to as space \mathcal{C}_2 [1, 2]. Some care is required to take into account the long range of dipole-dipole interaction. The usual way to compute the configurational energy U_{dd} is to replicate the basic simulation cell periodically in space and calculate U_{dd} as the sum of the interactions of the N dipoles in the basic cell with all the other dipoles in the cell and with the periodically repeated images in the surrounding cells

$$U_{dd} = \frac{\mu^2}{2} \sum_{i,j=1}^N \sum_{\mathbf{n}}' \left\{ \frac{\mathbf{s}_i \cdot \mathbf{s}_j}{|\mathbf{r}_{ij} + L\mathbf{n}|^2} - 2 \frac{[\mathbf{s}_i \cdot (\mathbf{r}_{ij} + L\mathbf{n})][\mathbf{s}_j \cdot (\mathbf{r}_{ij} + L\mathbf{n})]}{|\mathbf{r}_{ij} + L\mathbf{n}|^4} \right\} \quad (2)$$

The prime affixed to the sum over $\mathbf{n} = (n_x, n_y)$, with n_x, n_y integers, means that the term $i \neq j$ is omitted when $\mathbf{n} = 0$.

By a lattice summation technique (Ewald sum) the slowly and conditionally convergent sum is transformed into two rapidly convergent sums, one in direct space, the other in reciprocal space, the rate of convergence of both sums being regulated by the parameter α . The resulting expression for the energy of the 2D system is [1]

$$\begin{aligned} U_{dd} = & -\frac{\mu^2}{2} \sum_{i,j=1}^N \sum_{\mathbf{n}}' [b(|\mathbf{r}_{ij} + L\mathbf{n}|)\mathbf{s}_i \cdot \mathbf{s}_j \\ & + c(|\mathbf{r}_{ij} + L\mathbf{n}|)[\mathbf{s}_i \cdot (\mathbf{r}_{ij} + L\mathbf{n})][\mathbf{s}_j \cdot (\mathbf{r}_{ij} + L\mathbf{n})]] \\ & + \frac{\pi\mu^2}{S} \sum_{\mathbf{k} \neq 0} \frac{\exp(-k^2/4\alpha^2)}{k^2} F(\mathbf{k})F^*(\mathbf{k}) \\ & - \alpha^2 \mu^2 \sum_{i=1}^N \mathbf{s}_i^2 + \frac{\pi\mu^2}{2S} \left(1 - \frac{\epsilon' - 1}{\epsilon' + 1}\right) \left(\sum_{i=1}^N \mathbf{s}_i\right)^2, \end{aligned} \quad (3)$$

where the functions $b(r)$ and $c(r)$ are given by

$$b(r) = -\frac{\exp(-\alpha^2 r^2)}{r^2}, \quad (4)$$

$$c(r) = 2\left(\frac{1}{r^2} + \alpha^2\right) \frac{\exp(-\alpha^2 r^2)}{r^2}, \quad (5)$$

and

$$F(\mathbf{k}) = \sum_{i=1}^N (\mathbf{k} \cdot \mathbf{s}_i) \exp[i\mathbf{k} \cdot \mathbf{r}_i]. \quad (6)$$

In Eq. (3) $S = L^2$ is the area of the simulation cell, N the number of particles and F^* the complex conjugate of F . The wave-vectors \mathbf{k} which enter the reciprocal space contributions to the energy are of the form

$$\mathbf{k} = 2\pi\mathbf{n}/L. \quad (7)$$

Care has to be taken to properly choose the α parameter which governs the rate of convergence of the real- and reciprocal-space contributions in Eq. (3). It is generally taken sufficiently large so that only the terms with $\mathbf{n} = 0$ need to be retained in Eqs. (3). The last term in Eq. (3) represents the contribution to the energy from the depolarization field created when a continuous medium of dielectric constant ϵ' surrounds a disk shaped sample of periodic replica. For a conducting medium ($\epsilon' = \infty$) this term vanishes while for a system in vacuum ($\epsilon' = 1$) it is $\frac{\pi}{2S}\mathbf{M}^2$, where \mathbf{M} is the total polarization of the system.

A thermodynamic state of the DHD fluid is characterized by a reduced density $\rho^* = N\sigma^2/S$ where $S = L^2$ is the surface of the square of simulation and the reduced dipole μ^* with $\mu^{*2} = \mu^2/(k_B T \sigma^2)$ (k_B Boltzmann constant, T temperature).

B. Spherical boundary conditions

In this method the simulation cell is the surface of an ordinary sphere of center O and radius R , that will be referred to as space \mathcal{S}_2 [3, 4]. The electrostatics can be solved exactly in \mathcal{S}_2 in two different ways and therefore two distinct models are available [4, 6].

In the first version the DHD fluid is made of N ordinary (or mono-) dipoles $\boldsymbol{\mu}_i = \mu\mathbf{s}_i$ tangent to the sphere \mathcal{S}_2 at points $\mathbf{O}\mathbf{M}_i = R\mathbf{z}_i$ ($\mathbf{z}_i \cdot \mathbf{s}_i = 0$). In the second version considered in this article, one rather considers a collection of N bi-dipoles. A bi-dipole is defined as a dumbbell of two identical mono-dipoles located at two antipodal points of the sphere at points $\mathbf{O}\mathbf{M}_i = R\mathbf{z}_i$ and $\mathbf{O}\overline{\mathbf{M}}_i = -R\mathbf{z}_i$. The numerical experiments of Ref. [4] show that the convergence to the thermodynamic limit is in general faster for bi-dipoles than for mono-dipoles. The configurational energy of the DHD fluid reads

$$U(\{\mathbf{z}_i, \boldsymbol{\mu}_i\}) = \frac{1}{2} \sum_{i \neq j}^N v_{\text{HS}}^{\text{bi}}(\psi_{ij}) + \frac{1}{2} \sum_{i \neq j}^N W_{\boldsymbol{\mu}_i, \boldsymbol{\mu}_j}^{\text{bi}}, \quad (8)$$

where $v_{\text{HS}}^{\text{bi}}(\psi_{ij})$ is hard-core pair potential defined by

$$v_{\text{HS}}^{\text{bi}}(\psi_{ij}) = \begin{cases} \infty & \text{if } \sigma/R > \psi_{ij} \text{ or } \psi_{ij} > \pi - \sigma/R, \\ 0 & \text{otherwise,} \end{cases} \quad (9)$$

where ψ_{ij} is the angle between vectors \mathbf{z}_i and \mathbf{z}_j , *i.e.* $\cos \psi_{ij} = \mathbf{z}_i \cdot \mathbf{z}_j$ and thus $r_{ij} = R\psi_{ij}$ is the length of the geodesic length between points M_i and M_j . The dipole-dipole interaction $W_{\boldsymbol{\mu}_i, \boldsymbol{\mu}_j}^{\text{bi}}$ is given by

$$W_{\boldsymbol{\mu}_i, \boldsymbol{\mu}_j}^{\text{bi}} = \frac{\mu^2}{R^2} \frac{1}{\sin^2 \psi_{ij}} \left(\mathbf{s}_i \cdot \mathbf{s}_j + \frac{2 \cos \psi_{ij}}{\sin^2 \psi_{ij}} (\mathbf{s}_i \cdot \mathbf{z}_j)(\mathbf{s}_j \cdot \mathbf{z}_i) \right). \quad (10)$$

In Eq. (8) the vectors \mathbf{z}_i can always be chosen in the northern hemisphere \mathcal{S}_2^+ because of the special symmetries of the interaction. It is thus clear that the actual domain occupied by the fluid is the northern hemisphere \mathcal{S}_2^+ rather than the whole hypersphere. In terms of mono-dipoles the interpretation of the model is therefore the following : when a mono-dipole $\boldsymbol{\mu}_i$ leaves \mathcal{S}_2^+ at some point M_i of the equator the same dipole moment $\boldsymbol{\mu}_i$ reenters \mathcal{S}_2^+ at the antipodal point \overline{M}_i . Therefore bi-dipoles living on the whole sphere are equivalent to mono-dipoles living on the northern hemisphere but with special boundary conditions ensuring homogeneity and isotropy at equilibrium (in the case of a fluid phase). We stress that the expression (10) has been deduced rigorously from the solution of Laplace-Betrami equation in \mathcal{S}_2 [4] by contrast with the heuristic dipole-dipole interaction used in reference [3].

A thermodynamic state of this model is now characterized by a dimensionless number density $\rho^* = N\sigma^2/S$ where $S = 2\pi R^2$ is the 2D surface of the northern hemisphere \mathcal{S}_2 and the reduced dipole μ^* with $\mu^{*2} = \mu^2/(k_B T \sigma^2)$.

III. FULTON'S THEORY

Let us consider quite generally a polar fluid occupying a 2D surface Λ with boundaries $\partial\Lambda$. We assume the system to be at thermal equilibrium in a homogeneous and isotropic fluid phase. The fluid behaves macroscopically as a dielectric medium characterized by a scalar dielectric constant ϵ . Due to the lack of screening in such fluids, the asymptotic behaviour of the pair correlation function is long ranged and depends on the geometry of the system, *i.e.* its shape, size, and the properties imposed to the electric field (or potential) on the boundaries $\partial\Lambda$ as well. As a consequence, the expression of the dielectric constant

ϵ in terms of the fluctuations of polarization also depends on the geometry. These issues can be formally taken into account in the framework of Fulton's theory [7–9] which achieves an elegant synthesis between the linear response theory and the electrostatics of continuous media.

In addition to provide an expression for the dielectric constant ϵ Fulton's formalism also yields the asymptotic behaviour of the pair correlation function. Fulton's formalism can be extended without more ado to non-euclidian geometries and was applied notably to 3D cubic systems with periodic boundary conditions (space \mathcal{C}_3) and hyperspheres \mathcal{S}_3 in Refs. [6, 10], and, recently, to the 2D euclidian plane E_2 and the sphere \mathcal{S}_2 , for both mono- and bi-dipoles [4]. In this section we derive the missing results for space \mathcal{C}_2 and recall the results for 2D polar fluids in E_2 and \mathcal{S}_2 .

Fulton's relations constitute the quintessence of Fulton's formalism; they are formally independent of the geometry and read

$$\boldsymbol{\chi} = \boldsymbol{\sigma} + \boldsymbol{\sigma} \circ \mathbf{G} \circ \boldsymbol{\sigma} \quad (11a)$$

$$\mathbf{G} = \mathbf{G}_0 \circ (\mathbf{I} - \boldsymbol{\sigma} \circ \mathbf{G}_0)^{-1} \quad (11b)$$

Some comments seem appropriate. Let us first define the tensorial susceptibility $\boldsymbol{\chi}$. Under the influence of an external electrostatic field $\boldsymbol{\mathcal{E}}(\mathbf{r})$ the medium acquires a macroscopic polarization

$$\mathbf{P}(\mathbf{r}) = \langle \widehat{\mathbf{P}}(\mathbf{r}) \rangle_{\boldsymbol{\mathcal{E}}}, \quad (12)$$

where the brackets denote the equilibrium average of the microscopic polarization $\widehat{\mathbf{P}}(\mathbf{r}) = \sum_{j=1}^N \boldsymbol{\mu}_j \delta^{(2)}(\mathbf{r} - \mathbf{r}_j)$ in the presence of the external field $\boldsymbol{\mathcal{E}}$. The relation between the macroscopic polarization \mathbf{P} and the external field $\boldsymbol{\mathcal{E}}$ can be established in the framework of linear-response theory, provided that $\boldsymbol{\mathcal{E}}$ is small enough, with the result

$$2\pi\mathbf{P}(\mathbf{r}_1) = [\boldsymbol{\chi} \circ \boldsymbol{\mathcal{E}}](\mathbf{r}_1) \left(\equiv \int_{\Lambda} d^2\mathbf{r}_2 \boldsymbol{\chi}(\mathbf{r}_1, \mathbf{r}_2) \cdot \boldsymbol{\mathcal{E}}(\mathbf{r}_2) \right). \quad (13)$$

The r.h.s. of Eq. (13) has been formulated in a compact, albeit convenient notation that will be adopted henceforth, where the symbol \circ (which also enters Eqs. (11)) means both a tensorial contraction (denoted by the dot " \cdot ") and a spacial convolution over the whole domain Λ filled by the medium. The tensorial susceptibility $\boldsymbol{\chi}$ in Eq. (11a) reads

$$\boldsymbol{\chi}(\mathbf{r}_1, \mathbf{r}_2) = 2\pi\beta \langle \widehat{\mathbf{P}}(\mathbf{r}_1) \widehat{\mathbf{P}}(\mathbf{r}_2) \rangle, \quad (14)$$

where $\beta = 1/k_B T$ and the thermal averages are computed in the absence of the external field \mathcal{E} .

However, the dielectric properties of the fluid are characterized by the dielectric tensor ϵ . In Eqs (11) we have introduced, following Fulton, the convenient notation $\sigma = \epsilon - \mathbf{I}$ with $\mathbf{I}(\mathbf{r}_1, \mathbf{r}_2) = \mathbf{U}\delta^{(2)}(\mathbf{r}_{12})$ where $\mathbf{U} = \mathbf{e}_x\mathbf{e}_x + \mathbf{e}_y\mathbf{e}_y$ is the unit dyadic tensor. The tensor σ enters the constitutive relation

$$2\pi\mathbf{P} = \sigma \circ \mathbf{E} , \quad (15)$$

where the Maxwell field $\mathbf{E}(\mathbf{r})$ is the sum of the external field $\mathcal{E}(\mathbf{r})$ and the electric field created by the macroscopic polarization of the fluid. Therefore one has

$$\mathbf{E} = \mathcal{E} + 2\pi\mathbf{G}_0 \circ \mathbf{P} , \quad (16)$$

where \mathbf{G}_0 denotes the bare dipolar Green's function. Note that $2\pi\mathbf{G}_0(\mathbf{r}_1, \mathbf{r}_2) \cdot \boldsymbol{\mu}_2$ is the electric field at point \mathbf{r}_1 created by a point dipole $\boldsymbol{\mu}_2$ located at point \mathbf{r}_2 in vacuum and in the presence of the boundary $\partial\Lambda$. In the presence of the dielectric medium this field is now given by $2\pi\mathbf{G}(\mathbf{r}_1, \mathbf{r}_2) \cdot \boldsymbol{\mu}_2$ where the macroscopic, or dressed, Green's function is given by Eq. (11b) in which the inverse must be understood in the sense of operators.

It is generally assumed that ϵ is a local function, *i.e.* $\epsilon = \epsilon\mathbf{I}$. More precisely, it is plausible -and we shall take it for granted- that $\epsilon(\mathbf{r}_1, \mathbf{r}_2)$ is a short range function of the distance between the two points \mathbf{r}_1 and \mathbf{r}_2 , at least for a homogeneous liquid (or in the bulk in the presence of interfaces), and one then defines

$$\epsilon\mathbf{U} = \int_{\Lambda} d^2\mathbf{r}_2 \epsilon(\mathbf{r}_1, \mathbf{r}_2) . \quad (17)$$

Experiments show, and this fact must be admitted, that while ϵ is an intrinsic property of the medium Eqs. (11) show that the susceptibility tensor $\chi(\mathbf{r}_1, \mathbf{r}_2)$ is a long range function of \mathbf{r}_{12} which depends on the considered geometry. The locality assumption on ϵ allows an explicit calculation of the Green's function $\mathbf{G}(\mathbf{r}_1, \mathbf{r}_2)$ in some geometries, notably those used in MC simulations.

A. The square \mathcal{C}_2

In Ref. [10] Fulton's formalism was applied to the 3D dipolar hard sphere fluid in \mathcal{C}_3 . Here we will consider the 2D case which is a mere transposition so that we can skip many

details. Moreover we will consider only tinfoil boundary conditions, *i.e.* $\epsilon' = \infty$, which simplifies the algebra. The bare Green's function is given by

$$\mathbf{G}_0(\mathbf{r}_1, \mathbf{r}_1) \equiv \mathbf{G}_0(\mathbf{r}_{12}) = \frac{1}{2\pi} \frac{\partial}{\partial \mathbf{r}_{12}} \frac{\partial}{\partial \mathbf{r}_{12}} \psi(\mathbf{r}_{12}), \quad (18)$$

where $\psi(\mathbf{r})$ is the periodic Ewald potential. It satisfies Poisson's equation in \mathcal{C}_2

$$\Delta \psi(\mathbf{r}) = -2\pi [\delta_{\mathcal{C}_2}(\mathbf{r}) - \frac{1}{L^2}], \quad (19)$$

where

$$\begin{aligned} \delta_{\mathcal{C}_2}(\mathbf{r}) &= \sum_{\mathbf{n}} \delta^{(2)}(\mathbf{r} - L\mathbf{n}) \\ &= \frac{1}{L^2} \sum_{\mathbf{k}} \exp(i\mathbf{k} \cdot \mathbf{r}), \end{aligned} \quad (20)$$

is the periodical Dirac's comb. Expanding $\psi(\mathbf{r})$ and $\mathbf{G}_0(\mathbf{r})$ in Fourier series one finds

$$\psi(\mathbf{r}) = \frac{2\pi}{L^2} \sum_{\mathbf{k} \neq \mathbf{0}} \frac{\exp(i\mathbf{k} \cdot \mathbf{r})}{k^2} \quad (21a)$$

$$\mathbf{G}_0(\mathbf{r}) = -\frac{1}{L^2} \sum_{\mathbf{k} \neq \mathbf{0}} \widehat{\mathbf{k}} \widehat{\mathbf{k}} \exp(i\mathbf{k} \cdot \mathbf{r}), \quad (21b)$$

where $\widehat{\mathbf{k}} = \mathbf{k}/\|\mathbf{k}\|$.

It shall prove useful in what follows to remark that one can rewrite the Ewald potential as

$$\psi(\mathbf{r}) = -\log r + \frac{\pi}{2L^2} r^2 + \delta\psi(\mathbf{r}), \quad (22)$$

where $\delta\psi(\mathbf{r})$ is a harmonic function in the square and can thus be expressed quite generally as [11, 12]

$$\delta\psi(\mathbf{r}) = \sum_{m=1}^{\infty} a_m r^m \cos(m\varphi + \alpha_m), \quad (23)$$

where φ is the angle of \mathbf{r} with the axis \mathbf{e}_x and the constants a_m, α_m are such that $\psi(\mathbf{r})$ is a periodical function.

It is then easy to deduce from these prolegomena the two formulas

$$\text{Tr } \mathbf{G}_0(\mathbf{r}_1, \mathbf{r}_2) = \frac{1}{L^2} - \delta_{\mathcal{C}_2}(\mathbf{r}_{12}), \quad (24a)$$

$$2\widehat{\mathbf{r}}_{12} \cdot \mathbf{G}_0(\mathbf{r}_1, \mathbf{r}_2) \cdot \widehat{\mathbf{r}}_{12} = \frac{1}{L^2} + \frac{1}{\pi r_{12}^2} + \frac{1}{\pi} \sum_{m=2}^{\infty} m(m-1) a_m r^{m-2} \cos(m\varphi_{12} + \alpha_m). \quad (24b)$$

The computation of the dressed Green's function from its definition (11b) is conveniently made in Fourier space. Under the assumption of the locality of the dielectric tensor $\epsilon(\mathbf{r}_1, \mathbf{r}_2)$ one finds the obvious result $\mathbf{G} = \mathbf{G}_0/\epsilon$. Therefore Fulton's relation (11a) takes the explicit form

$$\chi(\mathbf{r}_1, \mathbf{r}_2) = (\epsilon - 1)\mathbf{I}(\mathbf{r}_1, \mathbf{r}_2) + \frac{(\epsilon - 1)^2}{\epsilon}\mathbf{G}_0(\mathbf{r}_1, \mathbf{r}_2). \quad (25)$$

We stress that the above equation has been obtained under the assumption of the locality of the dielectric tensor $\epsilon(\mathbf{r}_1, \mathbf{r}_2)$. Therefore it should be valid only asymptotically, *i.e.* for points $(\mathbf{r}_1, \mathbf{r}_2)$ at a mutual distance r_{12} larger than the range ξ of $\epsilon(\mathbf{r}_1, \mathbf{r}_2)$.

Taking the trace of Eq. (25), making use of Eq. (24a) and integrating both \mathbf{r}_1 and \mathbf{r}_2 over the square \mathcal{C}_2 one finds the expression of the dielectric constant

$$\epsilon - 1 = \frac{\pi\beta}{L^2} \langle \mathbf{M}^2 \rangle, \quad (26)$$

where $\mathbf{M} = \sum_{i=1}^N \boldsymbol{\mu}_i$ is the total dipole moment of the square.

We turn now our attention to the susceptibility tensor $\chi(\mathbf{r}_1, \mathbf{r}_2)$ which may be expressed in terms of the pair correlation function $g(1, 2)$ where $i \equiv (\mathbf{r}_i, \alpha_i)$ ($i = 1, 2$) denotes the position and the angle of dipole $\boldsymbol{\mu}_i$ with axis \mathbf{e}_x . One obtains that

$$\chi(\mathbf{r}_1, \mathbf{r}_2) = y\mathbf{I}(\mathbf{r}_1, \mathbf{r}_2) + 2y\rho \int_0^{2\pi} \frac{d\alpha_1}{2\pi} \int_0^{2\pi} \frac{d\alpha_2}{2\pi} h(1, 2)\mathbf{s}_1\mathbf{s}_2, \quad (27)$$

where $y = \pi\beta\rho\mu^2$ and $h = g - 1$ as usual. In the infinite plane E_2 the pair correlation function $g(1, 2)$ can be expanded on a complete set of rotational invariants among which the most important are

$$\Phi_{00}(1, 2) = 1, \quad (28a)$$

$$\Delta(1, 2) = \mathbf{s}_1 \cdot \mathbf{s}_2, \quad (28b)$$

$$D(1, 2) = 2(\mathbf{s}_1 \cdot \hat{\mathbf{r}}_{12})(\mathbf{s}_2 \cdot \hat{\mathbf{r}}_{12}) - \Delta(1, 2), \quad (28c)$$

where $\hat{\mathbf{r}}_{12} = \mathbf{r}_{12}/r_{12}$.

In space \mathcal{C}_2 the function $g(1, 2)$ has the symmetry of the square and *stricto sensu* cannot be expanded onto these rotational invariants. However, following de Leeuw *et al.*[13] one

defines the projections

$$h^\Delta(\mathbf{r}_{12}) = 2 \int_0^{2\pi} \frac{d\alpha_1}{2\pi} \int_0^{2\pi} \frac{d\alpha_2}{2\pi} h(1, 2) \Delta(1, 2), \quad (29a)$$

$$h^D(\mathbf{r}_{12}) = 2 \int_0^{2\pi} \frac{d\alpha_1}{2\pi} \int_0^{2\pi} \frac{d\alpha_2}{2\pi} h(1, 2) D(1, 2). \quad (29b)$$

$$(29c)$$

Note that the two projections $h^\Delta(\mathbf{r}_{12})$ and $h^D(\mathbf{r}_{12})$ are periodic functions which depend explicitly on the direction of vector \mathbf{r}_{12} . The susceptibility tensor $\chi(\mathbf{r}_1, \mathbf{r}_2)$ cannot be expressed in terms of these sole projections; however one can deduce from Eq. (27) and the definitions (29) the relations

$$\text{Tr} \chi(\mathbf{r}_1, \mathbf{r}_2) = 2y \delta_{c_2}(\mathbf{r}_{12}) + y \rho h^\Delta(\mathbf{r}_{12}), \quad (30a)$$

$$2\hat{\mathbf{r}}_{12} \cdot \chi(\mathbf{r}_1, \mathbf{r}_2) \cdot \hat{\mathbf{r}}_{12} = y \rho h^D(\mathbf{r}_{12}). \quad (30b)$$

The comparison of Eqs. (24), (30), and (25) yields the asymptotic behaviour of the projections $h^\Delta(\mathbf{r}_{12})$ and $h^D(\mathbf{r}_{12})$, *i.e.*, for $\|\mathbf{r}_{12}\| > \xi$. One has

$$h_{\text{asymp}}^\Delta(\mathbf{r}_{12}) = \frac{(\epsilon - 1)^2}{\epsilon} \frac{1}{y\rho} \frac{1}{L^2}, \quad (31a)$$

$$h_{\text{asymp}}^D(\mathbf{r}_{12}) = \frac{(\epsilon - 1)^2}{\epsilon} \frac{1}{y\rho\pi} \left\{ \frac{1}{r_{12}^2} + \sum_{m=2}^{\infty} m(m-1) a_m r_{12}^{m-1} \cos(m\varphi_{12} + \alpha_m) \right\}. \quad (31b)$$

In actual simulations one rather computes angular averages of the functions $h^\Delta(\mathbf{r}_{12})$ and $h^D(\mathbf{r}_{12})$, *i.e.*,

$$h^{\Delta(D)}(r_{12}) = \int_0^{2\pi} \frac{d\varphi_{12}}{2\pi} h^{\Delta(D)}(\mathbf{r}_{12}). \quad (32)$$

The asymptotic values of these averaged functions are simpler and given by

$$h_{\text{asymp}}^\Delta(r_{12}) = \frac{(\epsilon - 1)^2}{\epsilon} \frac{1}{y\rho} \frac{1}{L^2}, \quad (33a)$$

$$h_{\text{asymp}}^D(r_{12}) = \frac{(\epsilon - 1)^2}{\epsilon} \frac{1}{y\rho} \frac{1}{\pi r_{12}^2}, \quad (33b)$$

which are valid of course only for $\xi < r_{12} < L/2$. We note that, in the thermodynamic limit : *i.e.* for r fixed and $L \rightarrow \infty$, one recovers the expected Euclidian behaviours $h_{\text{asymp}}^\Delta(r) \sim 0$ (*i.e.* a short range function of r) and $h_{\text{asymp}}^D(r) \sim (\epsilon - 1)^2 / (\pi y \rho \epsilon) \times 1/r^2$ valid for the Euclidian plane E_2 without boundaries at infinity (cf. Refs. [3, 4]).

Our last comment concerns Eq. (26) which can be recast as

$$\epsilon - 1 = y \left\{ 1 + \frac{\rho}{2} \int_{\mathcal{C}_2} d^2\mathbf{r} h^\Delta(\mathbf{r}) \right\} \quad (34)$$

that we examine in the limit $L \rightarrow \infty$. We can then write

$$\epsilon - 1 = \left\{ 1 + \frac{\rho}{2} \int_{E_2} d^2\mathbf{r} h_\infty^\Delta(r) \right\} + \frac{\rho}{2} \int_{\mathcal{C}_2} d^2\mathbf{r} h_{\text{asympt}}^\Delta(r), \quad (35)$$

where we have noted that, in the limit $L \rightarrow \infty$, $h^\Delta(\mathbf{r}) \rightarrow h_\infty^\Delta(r)$ becomes an isotropic function. Making use of Eq. (33a) to compute the second integral in (35) one obtains

$$\frac{(\epsilon - 1)(\epsilon + 1)}{2\epsilon} = y \left\{ 1 + \frac{\rho}{2} \int_{E_2} d^2\mathbf{r} h_\infty^\Delta(r) \right\}. \quad (36)$$

This expression of ϵ is precisely that obtained in space E_2 by various methods [3, 4].

B. The sphere \mathcal{S}_2

We recall here the results of Ref. [4] for a fluid of bi-dipoles confined on the surface of the sphere \mathcal{S}_2 . The dielectric constant is given by

$$\frac{\epsilon - 1}{\epsilon} + \frac{(\epsilon - 1)^2}{2\epsilon} \cos \psi_0 = \mathbf{m}^2(\psi_0) \quad \text{with } 0 < \psi_0 < \pi/2, \quad (37)$$

where the fluctuation $\mathbf{m}^2(\psi_0)$ is given by

$$\mathbf{m}^2(\psi_0) = \frac{\pi\beta\mu^2}{S} \left\langle \sum_i^N \sum_j^N \mathbf{s}_i \cdot \mathbf{s}_j \Theta(\psi_0 - \psi_{ij}) \right\rangle, \quad (38)$$

with $S = 2\pi R^2$ (surface of the northern hemisphere) and $\Theta(x)$ the Heaviside step-function ($\Theta(x) = 0$ for $x < 0$ and $\Theta(x) = 1$ for $x > 0$). In the MC simulations reported in this paper we retained the optimal choice $\psi_0 = \pi/3$. Asymptotically (*i.e.* for a large fixed $r = R\psi \gg \xi$ and $\psi < \pi/2$), one has

$$h_{\text{asympt}}^\Delta(r) \sim -\frac{(\epsilon - 1)^2}{y\rho\epsilon} \frac{1}{2\pi R^2} \frac{1}{1 + \cos \psi}, \quad (39a)$$

$$h_{\text{asympt}}^D(r) \sim \frac{(\epsilon - 1)^2}{y\rho\epsilon} \frac{1}{2\pi R^2} \frac{1}{1 - \cos \psi}. \quad (39b)$$

As for \mathcal{C}_2 these asymptotic behaviours allow to recover from the formula (37) of the dielectric constant in space \mathcal{S}_2 the expression (36) in the thermodynamic limit.

IV. COMPARISONS OF THE TWO GEOMETRIES OF SIMULATION

We performed standard MC simulations of the DHD fluid in the canonical ensemble with single particle displacement moves (translation and rotation) in both geometries \mathcal{C}_2 and \mathcal{S}_2 . Some elements of comparison are given in Table I for three equilibrium states in the isotropic fluid phase of the model. We report values for the reduced internal energy per particle $\beta u = \langle \beta U_{dd} \rangle / N$, the contact values of the projections $g^{00}(\sigma)$, $h^\Delta(\sigma)$, and $h^D(\sigma)$ of the pair correlation function $g(1, 2)$, the compressibility factor $Z = \beta P / \rho$ (P the pressure) with $Z = Z_{HS} + \beta u$ and $Z_{HS} = 1 + (\pi \rho^* / 2) g^{00}(\sigma)$, and the specific heat $C_v / k_B = (\langle (\beta U_{dd})^2 \rangle - \langle \beta U_{dd} \rangle^2) / N$. As apparent in Table I, the agreement between the two methods of simulation is quite satisfactory. The values reported in the table were obtained for systems of $N \sim 1000$ particles for which $N_{\text{Conf.}} = 5 - 10 \times 10^6$ configurations per particle were generated. Note that the finite size scaling study of Ref. [4] gives, in the thermodynamic limit $N \rightarrow \infty$, $\beta u_\infty = -1.79000(6)$ for state ($\rho^* = 0.7$, $\mu^* = \sqrt{2}$) and $\beta u_\infty = -4.17138(15)$ for state ($\rho^* = 0.6$, $\mu^* = 2$), which shows that the data reported here are not very far from this limit.

We have also tested the validity of the asymptotic behaviours of $h^\Delta(r)$, and $h^D(r)$ in both geometries. We display in Fig. 1 these functions as well as their asymptotic behaviours (33) and (39) for the state ($\rho^* = 0.6$, $\mu^* = 2$). The values of the dielectric constant which enter these asymptotic behaviours are those given in Table. I. As apparent on the figures an excellent agreement between the MC data and the theoretical prediction is obtained. The small tails observed in $h^\Delta(r)$ at large r , which differ significantly in the two geometries, are of primary importance to ensure that the dielectric constants ϵ are identical in both geometries, within numerical uncertainties and finite size effects, although given by completely different formulas.

V. MC SIMULATIONS OF THE FLUID PHASE

The homogeneous, isotropic fluid phase is no more stable at low temperatures and complicated structures arise in this domain as indicated by some snapshots displayed in Fig. 2. At low densities, clusters of aligned dipoles, mostly organized into closed rings, appear at low temperatures and this topological structure becomes even more complex at higher densities.

In this low temperature regime the theory of the dielectric constant given in Sec. (III) becomes incorrect and the predicted asymptotic behaviours of $h^\Delta(r)$, and $h^D(r)$ are no more observed. Most probably the dielectric tensor, even if it exists, is no more isotropic and Fulton's theory breaks down. In order to establish the thermodynamic stability of the high temperature phase we have followed the authors of Ref.[14, 15] and computed the specific heat C_v as a function of μ for some densities $\rho^* = 0.05, 0.1, 0.2, 0.3, 0.4, 0.5, 0.6$, and 0.7 . A peak in $C_v(\mu)$ should be a signal of the "transition" or the limit of stability of the fluid phase. Some curves $C_v(\mu)$ are displayed in Fig. 3. They were obtained in the canonical ensemble for systems involving $N \sim 1000$ dipoles and runs of $N_{\text{Conf.}} = 5 - 10 \times 10^6$ configurations per particle. Table II provides the transition dipole moments for the different densities considered. In Ref [14] it has been pointed out that the polymerization transition may also be defined from the inflection point of $\Phi = N_p/N$ as a function of dipole moment (or temperature $T^* = 1/\mu^{*2}$) where N_p is the number of particles belonging to a cluster. At the density $\rho^* = 0.05$ where clusters are well defined we obtain a transition temperature in agreement with the value given in Table II.

VI. CONCLUSION

In this paper we have studied the 2D DHD system by means of MC simulations performed either in a square with periodic boundary conditions or on the surface of a sphere. The interactions between dipoles have been chosen so as to satisfy the laws of electrostatics in the two geometries. With this precaution both methods lead to identical results for the thermodynamic, structural and dielectric properties of the system, at least for sufficiently large systems. A subtlety in the asymptotic behaviours of the pair correlation function, strongly depending on the geometry, has been predicted and observed in the MC experiments performed in the isotropic fluid phase.

In the low temperature, low density part of the phase diagram a phase of living polymers of aligned dipoles organized into closed rings has been observed. At higher density the structure of this phase looks like an entangled structure of chains and rings.

At these low temperatures the laws of macroscopic dielectrics seem to be violated. A polymerization transition line based on the maximum of the specific heat as a function of dipole moment is provided. The critical dipole moment μ_c^* at the transition from fluid to

polymeric phase increases slightly with density.

We can contrast the present system with the one of 3D dipolar particles with centers of mass constrained to a monolayer or thin layer, at least if the dipoles are in-plane as it is the case at low temperatures. Such a quasi-two-dimensional (Q2D) system has been studied extensively in numerical simulations [5, 16–19] in view of its relevance to various experimental situations. References to experimental works can be found in [5, 16–19], see also Refs. [15, 20–23].

In Q2D systems the head to tail interaction of two particles at contact is $-2\mu^2$ and antiparallel side by side interaction is $-\mu^2$, while in 2D the interactions of both types of arrangement are of similar strength $-\mu^2$. One would therefore expect that chaining is much favoured in the Q2D case. This is easily demonstrated by comparing structural properties obtained in simulations of both systems. Notwithstanding, the overall qualitative structural behaviour appears to be much the same at comparable densities (and short range interaction), especially at low temperature, *i.e.*, formation of chains and rings. A notable difference between the Q2D and 2D systems is however that in the former system the spatial decay of the interaction is faster ($1/r^3$) than the system dimension ($D=2$) *i.e.*, of "short" range. Moreover, the angular dependence of the dipole-dipole interaction in Q2D systems is a linear combination of the 2D rotational invariants $D(1, 2)$ and $\Delta(1, 2)$.

Although 2D dipolar fluids do not exist *per se* in nature, the model could be used via various mappings for applications as, recently, for the hydrodynamics of two-dimensional microfluids of droplets. It is argued in Ref. [24] that droplet velocities show long-range orientational order decaying as $1/r^2$.

-
- [1] J. W. Perram and S. W. de Leeuw, *Physica* **109A**, 237 (1981).
- [2] G. P. Morriss and J. W. Perram, *Physica* **129A**, 395 (1985).
- [3] J.-M. Caillol, D. Levesque, and J.-J. Weis, *Mol. Phys.* **44**, 733 (1981).
- [4] J.-M. Caillol, [arXiv:1501.05538](https://arxiv.org/abs/1501.05538).
- [5] J.-J. Weis, J. M. Tavares, M. M. Telo da Gama, *J. Phys.: Condens. Matter* **14**, 9171 (2002).
- [6] J.-M. Caillol and M. Trulsson, *J. Chem. Phys.* **141**, 124111 (2014).
- [7] R. L. Fulton, *J. Chem. Phys.* **68**, 3089 (1978).
- [8] R. L. Fulton, *J. Chem. Phys.* **68**, 3095 (1978).
- [9] R. L. Fulton, *J. Chem. Phys.* **78**, 6865 (1983).
- [10] J.-M. Caillol, *J. Chem. Phys.* **96**, 7039 (1992).
- [11] J. D. Jackson, *Classical Electrodynamics* (John Wiley & Sons, New York, 1962).
- [12] B. Cichocki, B. U. Felderhof, and K. Hinsen, *Phys. Rev. A* **39**, 5450 (1989).
- [13] S. W. de Leeuw, J. W. Perram, and E. R. Smith, *Proc. R. Soc. London Ser. A* **373**, 27 (1980); **A 373**, 57 (1980). *Phys. Rev. A* **39**, 5450 (1989).
- [14] K. Van Workum and J.F. Douglas, *Phys. Rev. E* **71**, 031502 (2005).
- [15] J. Stambaugh, K. Van Workum, J.F. Douglas, and W. Losert, *Phys. Rev. E* **72**, 031301 (2005).
- [16] J.-J. Weis, *Mol. Phys.* **100**, 579 (2000).
- [17] J.-J. Weis, *J. Phys.: Condens. Matter* **15**, S1471 (2003).
- [18] S. Kantorovich, J. J. Cerdà, and Ch. Holm, *Phys. Chem. Chem. Phys.* **10**, 1883 (2008).
- [19] J. J. Cerdà, S. Kantorovich, and Ch. Holm, *J. Phys.: Condens. Matter* **20**, 204125 (2008).
- [20] K. Butter, P. H. Bomans, P. M. Frederik, G. J. Vroege, and A. P. Philipse, *J. Phys.: Condens. Matter* **15**, S1451 (2003)
- [21] K. Butter, P. H. Bomans, P. M. Frederik, G. J. Vroege, and A. P. Philipse, *Nat. Mater.* **2**, 88 (2003).
- [22] M. Klokkenburg, R. P. A. Dullens, W. K. Kegel, B. H. Ern e, and A. P. Philipse, *Phys. Rev. Lett.*, **86**, 037203 (2006).
- [23] J. Stambaugh, D. P. Lathrop, E. Ott, and W. Losert, *Phys. Rev. E* **68**, 026207 (2003).
- [24] I. Shani, T. Beatus, R. H. Bar-Ziv, and T. Tlusty, *Nature Physics*, **10**, 140 (2014).

geometry	ρ^*	μ^*	βu	Z	ϵ	$g^{00}(\sigma)$	$h^\Delta(\sigma)$	$h^D(\sigma)$	C_V/k_B
\mathcal{C}_2	0.7	$\sqrt{2}$	-1.789	3.990	17.45	4.346	2.826	4.578	.712
\mathcal{S}_2	0.7	$\sqrt{2}$	-1.790	3.974	17.83	4.339	2.814	4.575	.709
\mathcal{C}_2	0.6	2.0	-4.168	1.680	42.8	5.144	5.529	7.131	1.44
\mathcal{S}_2	0.6	2.0	-4.172	1.662	43.24	5.132	5.502	7.117	1.419
\mathcal{C}_2	0.1	2.0	-1.957	0.53	3.34	9.48	8.03	15.91	3.76
\mathcal{S}_2	0.1	2.0	-1.955	0.53	3.32	9.45	7.98	15.85	3.66

TABLE I: Geometry of simulation, dimensionless numerical density ρ^* , reduced dipole moment μ^* , reduced internal energy per particle βu , dielectric constant ϵ , compressibility factor $Z = \beta P/\rho$, contact values $g^{00}(\sigma)$, $h^\Delta(\sigma)$, and $h^D(\sigma)$ of some projections of the pair correlation function, and specific heat of the DHD fluid. For each state systems of $N = 1000$ particles were considered in \mathcal{S}_2 and $N = 1024$ in \mathcal{C}_2 . In both cases $N_{\text{Conf.}} = 5 - 10 \times 10^6$ configurations per particle were generated.

ρ^*	0.05	0.1	0.2	0.3	0.4	0.5	0.6
μ_c^*	2.35 ± 0.15	2.4 ± 0.1	2.5 ± 0.1	2.5 ± 0.25	2.6 ± 0.1	2.8 ± 0.1	3.0 ± 0.1

TABLE II: $\mu_c^*(\rho^*)$ for a system of $N = 1000$ dipolar hard disks.

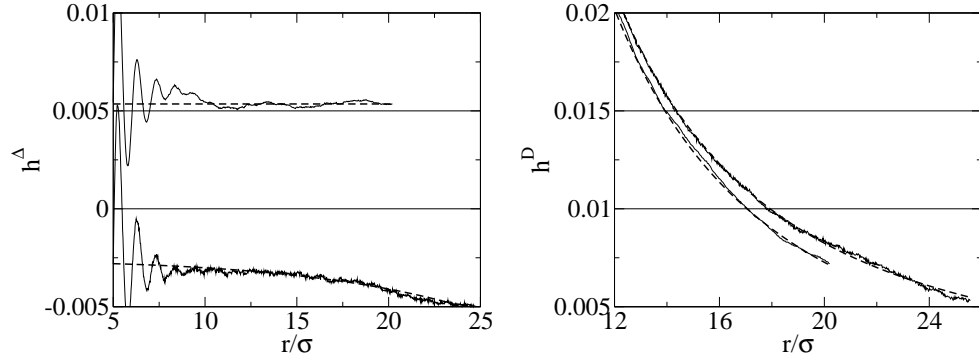


FIG. 1: Projections h^Δ (Top : \mathcal{C}_2 , bottom \mathcal{S}_2) and h^D (Top : \mathcal{S}_2 , bottom \mathcal{C}_2) for the state ($\rho^* = 0.6, \mu^* = 2$). Solid lines : MC data, dashed lines : predicted asymptotic behaviours. In space \mathcal{C}_2 : $r < L/2$ while in space \mathcal{S}_2 : $r < R\pi/2$.

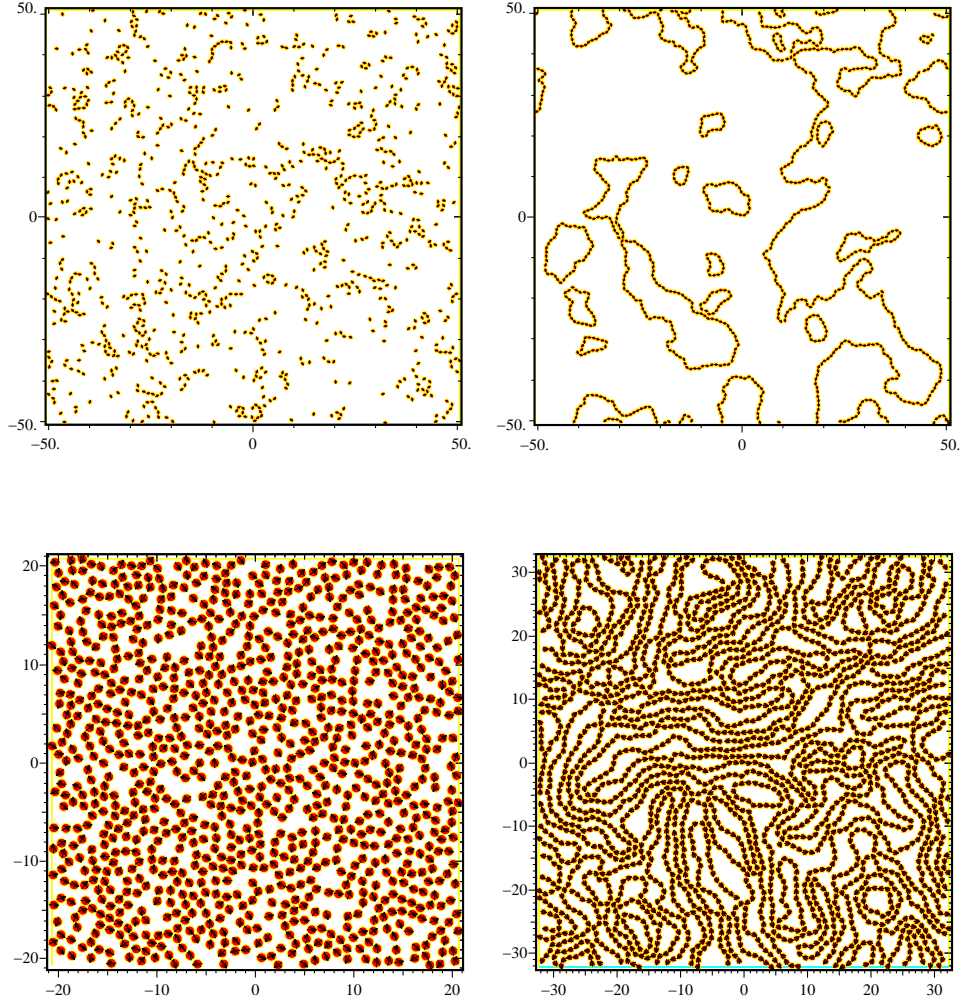


FIG. 2: Snapshots of configurations of the DHD system in space \mathcal{C}_2 . Top left : $(\rho^* = 0.1, \mu^* = 2, N = 1024)$, Top right : $(\rho^* = 0.1, \mu^* = 3, N = 1024)$, Bottom left : $(\rho^* = 0.6, \mu^* = 2, N = 1024)$, Bottom right : $(\rho^* = 0.6, \mu^* = 3.5, N = 2500)$.

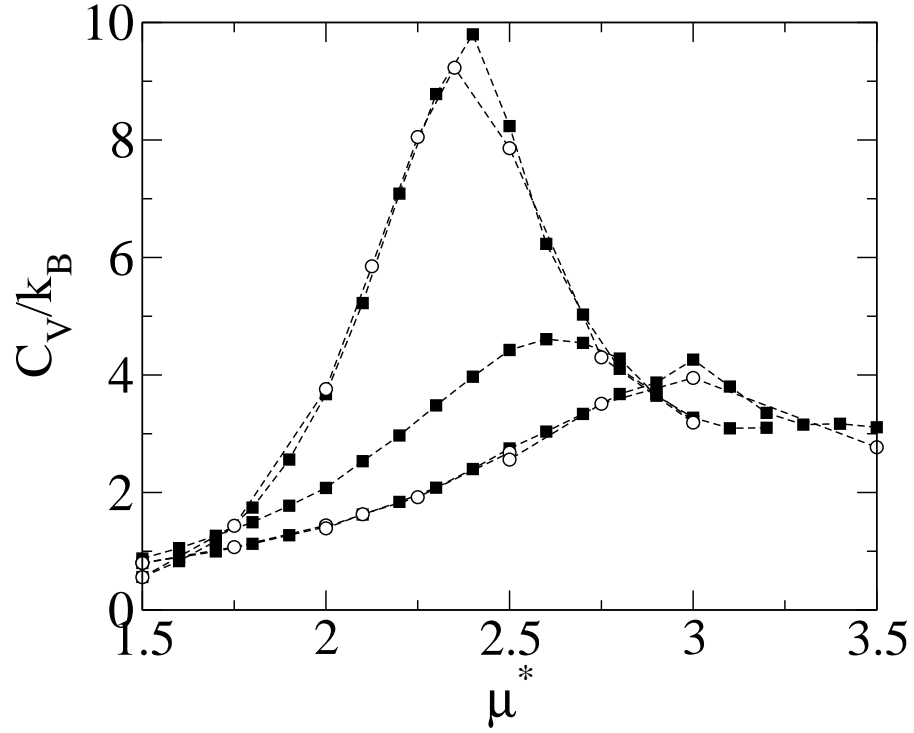


FIG. 3: Specific heat C_v/k_B versus reduced dipole moment μ^* . Solid squares : \mathcal{S}_2 , from left to right $\rho^* = 0.1, 0.4, 0.6$. Open circles : \mathcal{C}_2 , from left to right $\rho^* = 0.1, 0.6$. Dashed lines are guide lines for the eye.